Swarm Keeping Strategies for Spacecraft under J_2 and Atmospheric Drag Perturbations

Daniel Morgan[*] and Soon-Jo Chung[†]

University of Illinois at Urbana-Champaign, Urbana, IL, 61801, USA

Lars Blackmore[‡], Behcet Acikmese[§], David Bayard[¶] and Fred Y. Hadaegh[||]

Jet Propulsion Laboratory, California Institute of Technology, Pasadena, CA, 91109, USA

This paper presents several new open-loop guidance methods for spacecraft swarms comprised of hundreds to thousands of agents with each spacecraft having modest capabilities. These methods have three main goals: preventing relative drift of the swarm, preventing collisions within the swarm, and minimizing the fuel used throughout the mission. The development of these methods progresses by eliminating drift using the Hill-Clohessy-Wiltshire equations, removing drift due to nonlinearity, and minimizing the J_2 drift. In order to verify these guidance methods, a new dynamic model for the relative motion of spacecraft is developed. These dynamics are exact and include the two main disturbances for spacecraft in Low Earth Orbit (LEO), J_2 and atmospheric drag. Using this dynamic model, numerical simulations are provided at each step to show the effectiveness of each method and to see where improvements can be made. The main result is a set of initial conditions for each spacecraft in the swarm which provides hundreds of collision-free orbits in the presence of J_2. Finally, a multi-burn strategy is developed in order to provide hundreds of collision free orbits under the influence of atmospheric drag. This last method works by enforcing the initial conditions multiple times throughout the mission thereby providing collision free motion for the duration of the mission.

Nomenclature

A	cross sectional area of chief spacecraft
C_d	drag coefficient
CF	collision fraction
D	drift of spacecraft
$\bar{D}$	average drift of swarm
$\vec{F}$	drag force on chief spacecraft
J_2	second harmonic coefficient of Earth
$N(\nu, \sigma)$	Normal distribution with mean ν and standard deviation σ
Q_n	generalized force corresponding to q_n
R_e	radius of the Earth
$\vec{V}$	velocity of chief spacecraft
$\vec{V_a}$	velocity of chief spacecraft relative to atmosphere
X	collision distance
$(\hat{X}, \hat{Y}, \hat{Z})$	ECI coordinate system

[*]Graduate Research Assistant, Department of Aerospace Engineering, morgan29@illinois.edu, AIAA Student Member

[†]Assistant Professor, Department of Aerospace Engineering, sjchung@illinois.edu, AIAA Senior Member

[‡]Staff Engineer, Guidance and Control Analysis Group, james.c.blackmore@jpl.nasa.gov, AIAA Member

[§]Senior Member of the Technical Staff, Guidance and Control Analysis Group, behcet.acikmese@jpl.nasa.gov, AIAA Senior Member

[¶]Senior Research Scientist, Guidance and Control Analysis Group, david.bayard@jpl.nasa.gov, AIAA Associate Fellow

[||]JPL Fellow and Senior Research Scientist, Guidance and Control Analysis Group, fred.y.hadaegh@jpl.nasa.gov, AIAA Fellow

$\vec{a}_{drag}$	drag acceleration vector
h	angular momentum
i	orbit inclination
k_{J2}	$\frac{3}{2}J_2\mu R_e^2$, 2.633×10^{10} [km^5/s^2]
$\vec{l}$	relative position vector
$\dot{\vec{l}}$	relative velocity vector
m	mass of spacecraft
n	number of spacecraft
q_n	generalized coordinate
r	geocentric distance
r_{jZ}	distance from spacecraft to equator
$\vec{r}$	position vector of chief spacecraft
t	time
v_x	radial velocity
(x, y, z)	coordinate values in the LVLH coordinate system
$(\hat{x}, \hat{y}, \hat{z})$	unit vectors of the LVLH coordinate system
$(\hat{x}', \hat{y}', \hat{z}')$	unit vectors of the intermediate LVLH coordinate system
$(\hat{x}'', \hat{y}'', \hat{z}'')$	unit vectors of the J_2 aligned LVLH coordinate system
Ω	right ascension of the ascending node
α	rotation angle between $(\hat{x}, \hat{y}, \hat{z})$ and $(\hat{x}', \hat{y}', \hat{z}')$
β	rotation angle between $(\hat{x}', \hat{y}', \hat{z}')$ and $(\hat{x}'', \hat{y}'', \hat{z}'')$
δ	difference in a parameter between two spacecraft
μ	gravitational constant, 398600.4418 [km^3/s^2]
ρ	air density for chief spacecraft
θ	argument of latitude
ω_x	rotation rate of coordinate system about x-axis
ω_y	rotation rate of coordinate system about y-axis
ω_z	rotation rate of coordinate system about z-axis
$\vec{\omega}$	rotation vector of coordinate system
$\vec{\omega}_e$	rotation vector of Earth

Subscripts

0	initial condition (t = 0)
CP	concentric PRO condition
$J2$	parameter after accounting for J_2 terms
L	linearized condition
N	nonlinear condition (main result)
PM	period matched condition
j	parameter of deputy spacecraft ($j \leq n$)
r	desired condition of deputy spacecraft

I.   Introduction

Formation flying spacecraft have been a major area of research over the past decade due to their ability to perform certain tasks, such as interferometry[1] and distributed sensing,[2] and their potential to achieve performance at a cheaper cost than monolithic spacecraft. An expensive monolithic spacecraft can be replaced by many low cost spacecraft. Another advantage of formation flying (FF) spacecraft is that the formation as a whole is more redundant than a monolithic spacecraft because the failure of a single spacecraft in the formation can be overcome by the rest of the formation whereas the failure of a monolithic spacecraft most likely results in the failure of the mission. One of the main challenges of FF spacecraft is the Guidance, Navigation, and Control (GN&C) of the formation. As a result, a substantial amount of research has been done on the GN&C of FF spacecraft[3–11] in the last decade.

This paper is concerned with the GN&C of a challenging type of formation flying, spacecraft swarms. We define a swarm as a collection of 1000 or more spacecraft with masses on the order of 100g.[12] These swarms have potential for use as optical relays, distributed antennas, or for massively distributed sensing

American Institute of Aeronautics and Astronautics

applications among others. Ongoing research in microfabrication is developing the technologies required to fabricate, at low cost-per-unit, a 100g class of spacececraft, called femtosats, that can be actively controlled in all six degrees of freedom.[12]

The large increase in the number of spacecraft (two orders of magnitude larger than typical FF) and the small size of each spacecraft create several key challenges in spacecraft swarm control. The main challenge is the large increase in the probability of collisions caused by having so many spacecraft in such a small volume. Additionally, fuel efficiency becomes much more important because the size of the each spacecraft will limit the amount of fuel that can be carried by each spacecraft. One way to eliminate the need for complex controllers is to use J_2 invariant relative orbits, where the relative distance between spacecraft will be constant, thereby dramatically reducing the possibility of collisions. Another benefit of J_2 invariant relative orbits is that they are more fuel efficient than other orbits because they do not require corrections to account for J_2 drift. Even when J_2 drift is eliminated, atmospheric drag will cause the spacecraft to drift apart. One of the biggest problems when accounting for these perturbations, especially atmospheric drag, is the lack of an exact relative dynamic model including perturbations.

There are many dynamic models in the literature but each of them has limitations. For spacecraft separations on the order of hundreds of meters, the Hill-Clohessy-Wiltshire (HCW) equations have been shown to be good linear approximations of the relative dynamics,[13] with the added advantage that the resulting linear time invariant system has a closed form solution. In addition to assuming small separations from the reference orbit, the HCW equations also assume a circular reference orbit around a perfectly spherical, and homogeneous Earth. These assumptions can lead to large errors in the motion predicted by the HCW equations. There have been many attempts to develop more exact dynamics by removing some of the assumptions made in the HCW equations. Tschauner and Hempel[14] removed the restriction of circular orbits and developed the linear equations of motion for any orbit around a spherical Earth. Schweigart and Sedwick[15] developed linearized dynamics which include J_2 effects and Hamel and Lafontaine[16] extended this work to include eccentric orbits. Although these dynamic models are more accurate than the HCW equations, the linearization of the dynamics induces large errors when spacecraft separations are large. The relative dynamics have also been derived in the form of a state transition matrix.[17] If the initial states of an orbit are known, the state transition matrix can be used to find the states at any given time. The main drawback of this approach is that the state transition matrix has a complicated form, which makes it difficult to use. Exact nonlinear dynamics, which include the J_2 perturbation, were developed by Xu and Wang.[18] Chang *et al.*[19] derived an exact nonlinear dynamic model which includes both J_2 and atmospheric drag. However, the dynamics for the chief use classical orbital elements, which might make the implementation of the dynamic model more complicated. Therefore, this paper takes the method used by Xu and Wang[18] and extends it to include atmospheric drag in addition to J_2 effects using hybrid orbital elements. This produces an exact dynamic model which includes the major perturbations experienced by spacecraft in LEO. The derivation of this dynamic model can be found in Appendices A-B.

Several papers have attempted to find J_2 invariant relative motion between two spacecraft. The most popular method for finding these orbits is to set the differential mean orbital elements equal to zero using Gauss's variational equations (GVEs) to propagate the change in each spacecraft's orbital elements.[6–9] Breger *et al.*[10] found partial J_2 invariant orbits using the state transition matrix[17] and optimized the motion for minimum drift and fuel. Then, Breger and How[11] developed new linear time varying relative equations of motion and applied an online, model predictive controller to these dynamics. The methods developed by using GVEs and mean orbital elements are limited by the fact that they are designed for formations of ten or fewer spacecraft; however, the number of spacecraft in a swarm as well as the limited capability of each spacecraft creates several problems, which these controllers were not designed to handle. Mainly, the number of possible collisions scales quadratically with the number of spacecraft so in a swarm of thousands of spacecraft there are hundreds of thousands of possible collisions. This makes path planning and control a much more difficult problem.

In this paper, swarm keeping means maintaining relative distances between multiple spacecraft in the presence of disturbances and ensuring that collisions do not occur. The swarm keeping methods considered in this paper are motivated by four increasingly more realistic and complex dynamic models: (i) linearized dynamics given by the HCW equations, (ii) Keplerian dynamics with spherical Earth assumptions, (iii) exact dynamics with J_2,[18] and (iv) exact dynamics with J_2 and atmospheric drag (derived in Appendix A-B). Furthermore, regardless of which model is used to motivate the swarm keeping method, each method is evaluated using dynamic models (ii) and (iii), except in Section V where atmospheric drag is considered

and dynamic model (iv) is used.

The main contribution of this paper is the investigation of various methods of swarm keeping and using numerical simulations to show the effectiveness of each method. Energy matching conditions are introduced in Section IV as a method for swarm keeping with respect to J_2 influence.[20] Energy matching is shown by simulation, in the presence of J_2, to provide collision free swarm motion for several hundred orbits with only a single initializing burn by each agent. Related work has found other conditions that prove J_2 invariance under certain restricted orbits.[6–10] In comparison, simulations in Section IV suggest that energy matching provides a powerful method to minimize both swarm drift rate and the collision rate across a wide range of reference orbits regardless of altitude, eccentricity, and inclination. A main contribution of this paper is to identify energy matching as a very effective approach to swarm keeping. In Section V, a multi-burn guidance method is developed and implemented which extends the energy matching method so that it is effective in the presence of atmospheric drag in addition to J_2. The collision free equations and multi-burn guidance method are designed specifically to address the major concerns of spacecraft swarm GN&C, including collision avoidance and fuel efficiency.

The paper is organized as follows. In Section II, we describe the problem statement and the assumptions made in initializing the swarm. Additionally, we define the metrics that are used to quantify the swarm motion. In Section III, we investigate the effect of J_2 on the swarm and use the HCW equations to develop some simple single burn control options. In Section IV, we present the main results by expanding upon the equations developed in Section III taking into account the J_2 perturbation. In Section V, we rerun the simulations with atmospheric drag and use a multi-burn guidance method based on the equations developed in Section IV in order to provide collision free motion in an environment perturbed by both J_2 and drag. The simulations run in this paper use an exact dynamic model including J_2 and atmospheric drag. The derivation for this model is located in Appendix A-B.

II.   Preliminaries: Swarm Initialization

In order to investigate the relative motion of the swarm, two coordinate systems must be defined. First, the Earth Centered Inertial (ECI) coordinate system is used to locate the chief spacecraft or a virtual reference point called the chief orbit (see Fig. 1a). This coordinate system is fixed and located at the center of the Earth. The $\hat{X}$ direction points towards the vernal equinox, the $\hat{Z}$ direction points towards the north pole, and the $\hat{Y}$ direction is perpendicular to the other two and completes the right-handed coordinate system. The second coordinate system is the Local Vertical, Local Horizonal (LVLH) coordinate system. The LVLH frame is centered at the chief spacecraft or chief orbit. Figure 1a shows the LVLH frame with respect to a chief spacecraft. The $\hat{x}$, or radial, direction is always aligned with the position vector and points away from the Earth, the $\hat{z}$, or crosstrack, direction is aligned with the angular momentum vector, and the $\hat{y}$, or alongtrack, direction completes the right-handed coordinate system. The LVLH frame is a rotating frame with a rotation rate of ω_x about the radial axis and ω_z about the crosstrack axis. In other words, ω_x is the precession rate of the coordinate system and ω_z is the orbital rotation rate.

The chief orbit is defined using hybrid orbital elements which include: geocentric distance (r), radial velocity (v_x), angular momentum (h), inclination (i), right ascension of the ascending node (Ω), and argument of latitude (θ). These six parameters fully define[18] the chief orbit in the ECI frame. These hybrid states are used instead of the classical orbital elements because the orbits of the spacecraft may vary due to the perturbations. Hybrid states still have a physical meaning when describing a perturbed orbit. The classical orbital elements can easily be found from the hybrid states. The exact dynamics for the chief orbit are derived in Appendix A. Now that the chief orbit has been located, we can define the LVLH frame for the chief orbit and use it to locate the deputy spacecraft. The relative position and velocity of the deputy spacecraft are expressed by $\vec{l}_j = [\, x_j \quad y_j \quad z_j \,]^T$ and $\dot{\vec{l}}_j = [\, \dot{x}_j \quad \dot{y}_j \quad \dot{z}_j \,]^T$, respectively.

For numerical simulations in this paper, the initial distribution of the swarm is a normal distribution in each direction. Each normal distribution is centered at the chief, or origin of the LVLH frame, and has a standard deviation σ. In other words, the initial position of a spacecraft can be written as $(x, y, z) = (N(0, \sigma), N(0, \sigma), N(0, \sigma))$ where all normal distributions are independent. This distribution was chosen to represent a random deployment of the swarm. The actual deployment of the spacecraft would need to be more controlled than what is assumed for the simulations in this paper. Therefore, the results in the following sections give conservative estimates for the number of collisions. Additionally, each deputy has the same velocity as the chief in the LVLH frame which means that $(\dot{x}, \dot{y}, \dot{z}) = (0, 0, 0)$. However, in all of the

American Institute of Aeronautics and Astronautics

(a) ECI ($\hat{X}, \hat{Y}, \hat{Z}$) and LVLH Frames ($\hat{x}, \hat{y}, \hat{z}$)
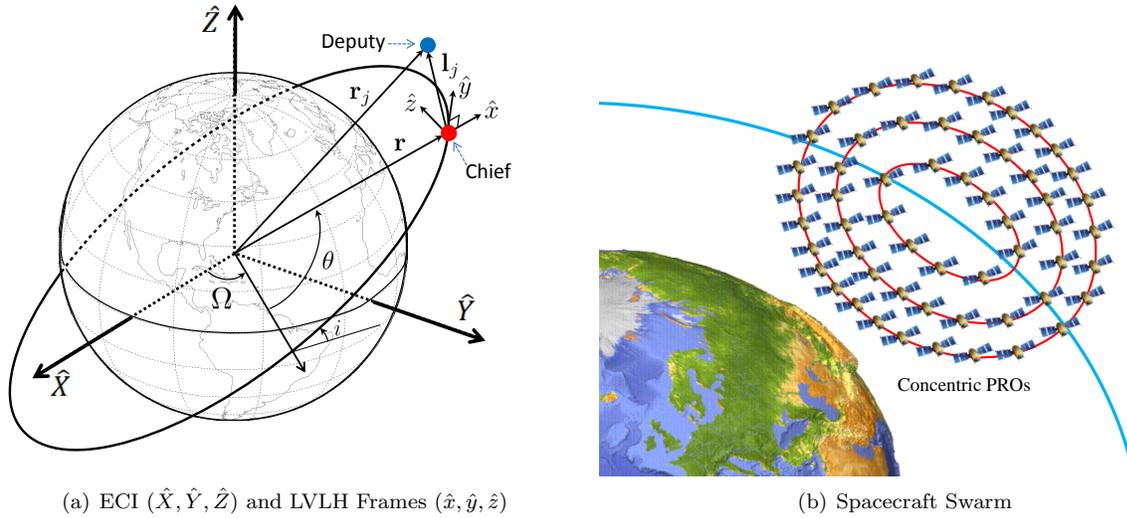
(b) Spacecraft Swarm

Figure 1. A visualization of the relative coordinate system and a spacecraft swarm

simulations, each spacecraft performs a burn at the start of the simulation so the assumption that all of the relative velocities are the same will not affect the swarm motion. An example of a spacecraft swarm is shown in Fig. 1b.

Each simulation in this paper is run for a period of 500 orbits with 60 output times per orbit. Unless otherwise specified, the nominal swarm has a circular chief orbit with an altitude of 500 km, an inclination of 45 degrees, and an argument of latitude of 45 degrees. The nominal swarm has 500 deputies distributed around the chief using a standard deviation (σ) of 0.5 km.

In order to determine the effectiveness of a swarm, we define metrics to quantify the motion of the swarm. Two metrics are the drift of each spacecraft (D_j) and the average drift of the swarm ($\bar{D}$). The drift of a spacecraft is the maximum alongtrack position in the LVLH frame over all orbits compared to the maximum alongtrack position attained during its first orbit, and is illustrated in Fig. 2. The average drift of the swarm is shown in the following equation.
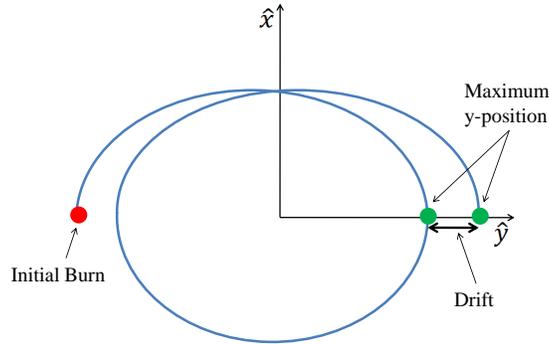
Figure 2. Drift of a Spacecraft

$$\bar{D} \triangleq \frac{1}{n} \sum_{j=1}^{n} D_j \tag{1}$$

The collision fraction of the swarm is defined as the number of spacecraft which have come within a distance X of another spacecraft at, or before, a given time. The definition of collision fraction (CF) is shown below.

American Institute of Aeronautics and Astronautics

$$R_j(t') \triangleq \begin{cases} 0 \text{ if } \|\vec{l}_j(t) - \vec{l}_i(t)\| > X \text{ for all } t \leq t' \text{ and all } i \neq j \\ 1 \text{ if } \|\vec{l}_j(t) - \vec{l}_i(t)\| \leq X \text{ for any } t \leq t' \text{ and any } i \neq j \end{cases} \tag{2}$$

$$CF(t) \triangleq \frac{1}{n} \sum_{j=1}^{n} R_j(t) \tag{3}$$

where n is the number of spacecraft, t is the time vector, and t' is a specific time point in t. Then, we define physical collisions by setting $X = 1$ m. It is important to note that once a spacecraft collides, it continues on the same trajectory and can collide with other spacecraft. However, the collision fraction measures how many of the spacecraft have collided. Therefore, this metric is always between 0 and 1 and is always increasing. A collision fraction of 0 means the swarm is collision free at that time and a collision fraction of 1 means that all spacecraft have collided at least once before that time.

III.   Single Burn Swarm Keeping Options

This section investigates the relative dynamics of spacecraft swarms in a J_2 perturbed orbit by allowing each spacecraft to execute a single burn at time $t = 0$. Since the spacecraft are initialized with no relative velocity, the ΔV required for each burn is equal to the velocity at $t = 0^+$. Another way to look at this problem is that we are setting the initial conditions for each spacecraft and then numerically integrating the exact dynamics with J_2 only. For each simulation, we are looking at three parameters: average drift ($\bar{D}$), fuel required for the initial burn (ΔV), and collision fraction (CF). Average drift shows whether or not the swarm is maintaining its original shape and how fast the swarm is dispersing, fuel required tells us how expensive each option is, and collision fraction tells us how many of the spacecraft are collision free at a given time. In an ideal scenario, all of these parameters will be small. The initial burns discussed in the following subsections begin with the simplest, most fuel efficient approach, and become increasingly more complex while demonstrating better drift and collision results. The purpose of this section is to provide some simple control methods to use as a benchmark for the main result which is developed in Section IV.

A.   Uncontrolled Motion

Although we know that the J_2 disturbance will cause the chief orbit to drift relative to the Keplerian orbit, it is unknown how the spacecraft will move relative to each other. For most applications, the motion of the swarm as a whole can be perturbed as long as the swarm itself maintains its shape. We know that spacecraft with different orbital periods will rapidly drift apart. In fact, running simulations for spacecraft with different periods shows that the drift rate of the swarm is on the order of tens of km/orbit.

B.   Period Matching

1.   Linearized Period Matching

In order to reduce the drift rate of the swarm, we first eliminate the drift caused by differences in the orbital periods of each spacecraft. Since the spacecraft are initialized at a position which is within a few kilometers of the chief orbit, we can use the HCW equations to find the initial conditions required for period matching with the only additional constraint being a circular chief orbit. The solution to the HCW equations, which give the relative position and velocity of the spacecraft as functions of time, are shown below:[13]

$$\begin{bmatrix} x(t) \\ y(t) \\ z(t) \\ \dot{x}(t) \\ \dot{y}(t) \\ \dot{z}(t) \end{bmatrix} = \begin{bmatrix} 4 - 3\cos\omega_z t & 0 & 0 & \sin\omega_z t/\omega_z & 2(1 - \cos\omega_z t)/\omega_z & 0 \\ 6\sin\omega_z t - 6\omega_z t & 1 & 0 & 2(-1 + \cos\omega_z t)/\omega_z & 4\sin\omega_z t/\omega_z - 3t & 0 \\ 0 & 0 & \cos\omega_z t & 0 & 0 & \sin\omega_z t/\omega_z \\ 3\omega_z \sin\omega_z t & 0 & 0 & \cos\omega_z t & 2\sin\omega_z t & 0 \\ 6\omega_z(-1 + \cos\omega_z t) & 0 & 0 & -2\sin\omega_z t & -3 + 4\cos\omega_z t & 0 \\ 0 & 0 & -\omega_z \sin\omega_z t & 0 & 0 & \cos\omega_z \end{bmatrix} \begin{bmatrix} x_0 \\ y_0 \\ z_0 \\ \dot{x}_0 \\ \dot{y}_0 \\ \dot{z}_0 \end{bmatrix} \tag{4}$$

The only terms that are secular are the ones which are multiplied by t in Eq. (4). These terms are responsible for the majority of the drift described in Section III.A. Therefore, if we set the sum of these terms to zero, we will reduce the drift from the previous simulation. Setting these terms to zero yields the conditions:

$$\dot{x}_{0,L,PM} = 0, \quad \dot{y}_{0,L,PM} = -2\omega_z x_0, \quad \dot{z}_{0,L,PM} = 0 \tag{5}$$

Since the HCW equations are used, we are assuming an unperturbed circular reference orbit and the orbital rotation rate is defined by $\omega_z = \sqrt{\mu/r^3}$.

Equation (5) are the linearized conditions required for period matching the swarm, indicated by the subscript (L,PM). Period matching results in the second condition in Eq. (5) and the first and third conditions are chosen in order to minimize fuel. Equation (5) assumes that all of the spacecraft have the zero relative velocity upon deployment. If this is not the case, then the first and third conditions can be modified so that the change in radial and crosstrack velocity is zero. In Section IV, all three conditions will be fully defined, which will eliminate this dependency on the initial velocities. The simulation results for a linearized period matched swarm are shown in Fig. 3.

(a) Drift results   (b) Collision results
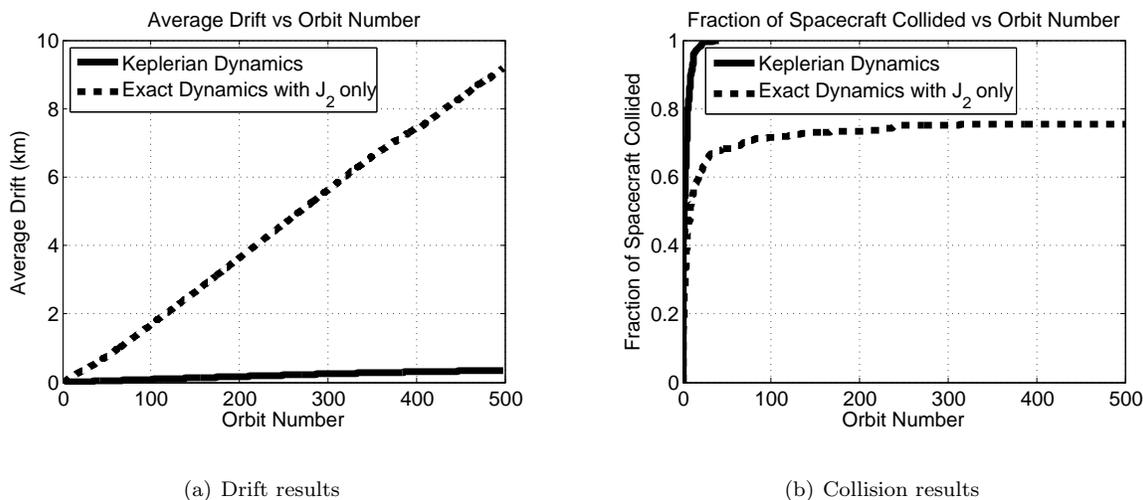
Figure 3. Simulation results of a linearized period matched swarm

In Fig. 3a, the drift using Keplerian dynamics is nearly zero. The small drift is caused by the fact that Eq. (4) is the linearized solution but the simulation is run using the Keplerian dynamics, which are nonlinear. Now that the drift has been reduced, the effect of the J_2 perturbation is evident. The drift rate under exact dynamics with J_2 only is 18.4 m/orbit (over the first 500 orbits). This drift rate is about 1000 times less than the drift rate in the uncontrolled swarm. At this drift rate, the swarm size will no longer limit the swarm's functionality.

Unfortunately, there are some disadvantages to the period matched swarm. The first disadvantage is that the average ΔV required per spacecraft is 0.9 m/s. The second, and much more alarming, problem with this approach can be seen in Fig. 3b. This figure shows the collision results for the period matched swarm. Within the first few orbits, the collision fraction is above 0.5. This means that most of the spacecraft collide immediately and the rest collide shortly after. Therefore, these initial conditions are not sufficient for a functional swarm.

2. Nonlinear Period Matching (Energy Matching without J_2)

The linearized period matching results are only valid for small swarms with circular chief orbits. In order to eliminate the errors caused by the linearization and eccentric chief orbits, we match the energy of all spacecraft using Keplerian dynamics. Recall that the inertial velocity for the chief and deputy spacecraft are $\vec{V}$ and $\vec{V}_j$, respectively. Their definitions are shown below.

American Institute of Aeronautics and Astronautics

$$\vec{V} = v_x\hat{x} + \frac{h}{r}\hat{y} \tag{6}$$

$$\vec{V}_j = (v_x + \dot{x}_j - y_j\omega_z)\hat{x} + (\frac{h}{r} + \dot{y}_j + x_j\omega_z - z_j\omega_x)\hat{y} + (\dot{z}_j + y_j\omega_x)\hat{z} \tag{7}$$

The energy matching condition is shown below. $\|\vec{V}_r\|$ is the required deputy velocity magnitude for energy matching given the deputy position (r_j) and the chief position (r).

$$\frac{\|\vec{V}\|^2}{2} - \frac{\mu}{r} = \frac{\|\vec{V}_r\|^2}{2} - \frac{\mu}{r_j} \tag{8}$$

This equation can be rewritten as

$$\|\vec{V}_r\| = \sqrt{\|\vec{V}\|^2 + 2\mu\left(\frac{1}{r_j} - \frac{1}{r}\right)} \tag{9}$$

where $\vec{V}$ is given in Eq. (6). Next, we take the velocity resulting from the linearized initial conditions and apply the energy matching condition in the direction of the current velocity in order to minimize the amount of fuel used. The energy matching condition is shown below.

$$\vec{V}_{N,PM} = \frac{\|\vec{V}_r\|}{\|\vec{V}_{L,PM}\|}\vec{V}_{L,PM} \tag{10}$$

In this equation, $\vec{V}_{L,PM}$ is the velocity required to satisfy the linearized period matching conditions. This velocity is defined by substituting linearized initial conditions into Eq. (7) and results in the following equation.

$$\vec{V}_{L,PM} = (v_x + \dot{x}_{0,L,PM} - y_0\omega_z)\hat{x} + (\frac{h}{r} + \dot{y}_{0,L,PM} + x_0\omega_z - z_0\omega_x)\hat{y} + (\dot{z}_{0,L,PM} + y_0\omega_x)\hat{z} \tag{11}$$

Substituting Eq. (11) into Eq. (10) and solving for the initial conditions in the LVLH frame results in the following conditions for nonlinear period matching.

$$\dot{x}_{0,N,PM} = \frac{\|\vec{V}_r\|}{\|\vec{V}_{L,PM}\|}\dot{x}_{0,L,PM} + \left(\frac{\|\vec{V}_r\|}{\|\vec{V}_{L,PM}\|} - 1\right)(v_x - y_0\omega_z)$$

$$\dot{y}_{0,N,PM} = \frac{\|\vec{V}_r\|}{\|\vec{V}_{L,PM}\|}\dot{y}_{0,L,PM} + \left(\frac{\|\vec{V}_r\|}{\|\vec{V}_{L,PM}\|} - 1\right)\left(\frac{h}{r} + x_0\omega_z - z_0\omega_x\right) \tag{12}$$

$$\dot{z}_{0,N,PM} = \frac{\|\vec{V}_r\|}{\|\vec{V}_{L,PM}\|}\dot{z}_{0,L,PM} + \left(\frac{\|\vec{V}_r\|}{\|\vec{V}_{L,PM}\|} - 1\right)y_0\omega_x$$

The nonlinear period matched initial conditions can be found by substituting Eq. (5) into Eq. (12). This result is shown below.

$$\dot{x}_{0,N,PM} = \left(\frac{\|\vec{V}_r\|}{\|\vec{V}_{L,PM}\|} - 1\right)(v_x - y_0\omega_z)$$

$$\dot{y}_{0,N,PM} = \frac{\|\vec{V}_r\|}{\|\vec{V}_{L,PM}\|}(-2\omega_z x_0) + \left(\frac{\|\vec{V}_r\|}{\|\vec{V}_{L,PM}\|} - 1\right)\left(\frac{h}{r} + x_0\omega_z - z_0\omega_x\right) \tag{13}$$

$$\dot{z}_{0,N,PM} = \left(\frac{\|\vec{V}_r\|}{\|\vec{V}_{L,PM}\|} - 1\right)y_0\omega_x$$

Applying these initial conditions to the nominal swarm yields results very similar to those in Fig. 3 with the only difference being the fact that the nonlinear initial conditions eliminate the drift under Keplerian

American Institute of Aeronautics and Astronautics

dynamics. This is to be expected because we know that period matching is sufficient to eliminate drift assuming a spherical Earth. Under the influence of J_2, the nonlinear initial conditions in Eq. (13) have the same limitations as the linearized initial conditions in Eq. (5). Therefore, a new method which eliminates collisions within the swarm will be developed in Section IV.

In order to determine why these collisions happen, the motion of the swarm can be studied by looking at the passive relative orbits (PROs) of each spacecraft. The analysis of the PROs shows two important aspects of swarm motion. First, although the swarm is slowly expanding from the macroscopic perspective, the swarm agents are moving very quickly relative to each other. In other words, the swarm size is changing very slowly but its shape is rapidly changing. This would make it difficult for the swarm to perform an interferometry mission that requires a specific swarm configuration. The other aspect of swarm motion that was discovered is that the spacecraft's PROs are intersecting in the x-y plane of the LVLH frame and these intersection points are where the collisions are occurring. Figure 4 shows the projection of ten PROs in the x-y plane. In this figure, it is clear that many collisions can occur because there are many intersections between the ten orbits. Obviously, as the number of spacecraft increases to 500 or 1000, the number of possible collisions will increase rapidly. The reason for these intersections is the fact that each PRO has a different center point.
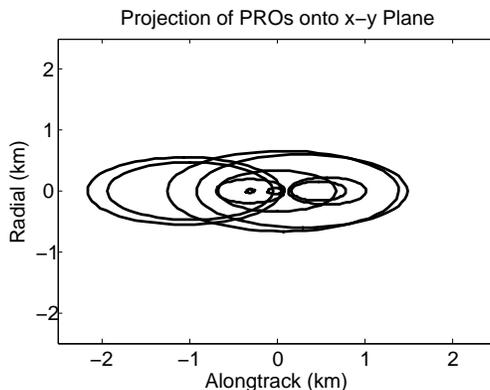
Figure 4. **The projection in the x-y plane of the first orbit for ten spacecraft in a period matched swarm**

C. Concentric PROs

1. Linearized Concentric PROs

As stated in the previous subsection, the reason for collisions is the fact that the PROs of the spacecraft are intersecting in the x-y plane of the LVLH frame. In order to prevent collisions, the spacecraft must be placed on concentric PROs. If the PROs are concentric, then any two spacecraft will either be on PROs that do not intersect because one is completely inside the other or they will be on the same PRO with one following the other. Either way the spacecraft cannot collide unless they are on the same PRO with the same phase but this can only happen if they are initialized at the same position, which is very unlikely. In order to find the initial conditions for concentric PROs, we once again look at the solutions to the HCW equations, which are shown in Eq. (4).

In addition to the initial condition required by Eq. (5), the constant terms in the $x(t)$ and $y(t)$ equations must be the same for all spacecraft in order for them to be on concentric PROs in the x-y plane. For simplicity, we set them equal to zero. The results are as follows:

$$\dot{x}_{0,L,CP} = \frac{1}{2}\omega_z y_0, \quad \dot{y}_{0,L,CP} = -2\omega_z x_0, \quad \dot{z}_{0,L,CP} = 0 \tag{14}$$

where the first two conditions come from the concentric PROs and the third condition is set to zero in order to minimize fuel. The third condition is based on the assumption that the spacecraft are initialized with no

American Institute of Aeronautics and Astronautics

relative velocity in the LVLH frame. Setting the constant terms to zero in the $x(t)$ equation results in the condition for period matching from Eq. (5), which means that any period matched spacecraft has a PRO centered at zero in the x direction. Therefore, we now have two initial conditions which will give us period matched orbits with PROs that will not intersect. The results of the concentric PRO swarm are shown in Fig. 5.

(a) Drift results

(b) Collision results
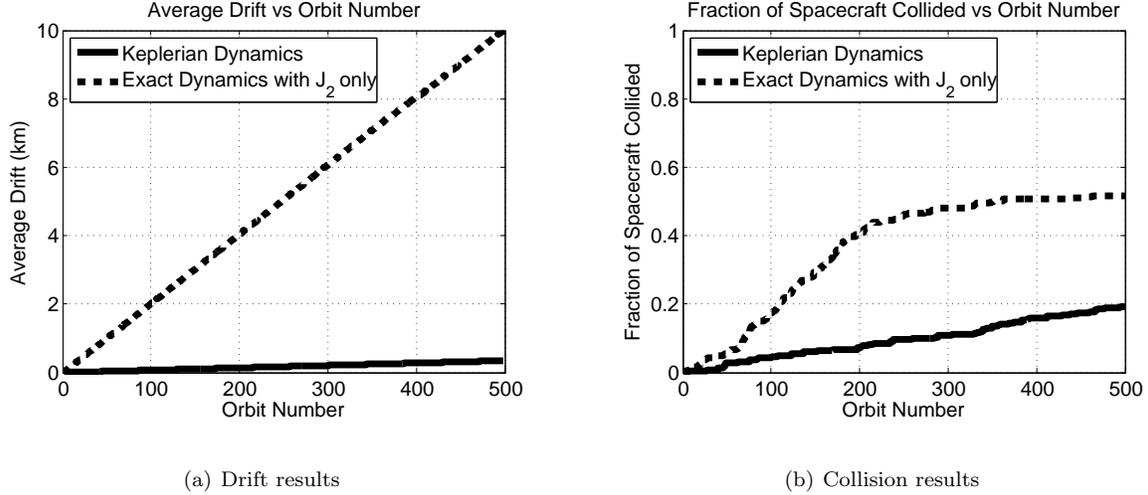
Figure 5. Simulation results of a linearized concentric PRO swarm

Figure 5a shows the drift results for the concentric PRO swarm. These results are nearly identical to the drift results from a period matched swarm. The drift rate of the swarm under the influence of J_2 is 20.0 m/orbit, which is small compared to the initial size of the swarm. The average fuel cost per spacecraft of this method is 1.1 m/s which is about a 25% increase compared to the period matched swarm.

On the other hand, the collision results in Fig. 5b show much improvement compared to the previous simulation. The concentric PRO swarm is nearly collision free (one or two collisions) for the first 60 orbits even with the exact dynamics with J_2 only. This collision free motion occurs because the PROs do not intersect in the x-y plane. Figure 6a shows the first orbit for ten spacecraft and it is clear that no collisions can occur. The collision free motion continues until somewhere between orbit 60 and orbit 200. At this time, more than half of the spacecraft collide. The reason for this large jump in collisions is that each PRO is slightly drifting due to the J_2 effect. The problem arises because the PROs are drifting at different rates and in different directions so eventually the PROs will intersect in the x-y plane at which time collisions start to occur. The PRO drift is illustrated in Fig. 6b.

2. Nonlinear Concentric PROs

As with the linearized period matching initial conditions, the linearized concentric PRO conditions assume circular chief orbits and small swarms. Therefore, some linearization errors occur when these initial conditions are used with the Keplerian dynamics even though no perturbations are included. In order to eliminate these errors we use the same energy matching method as we did in Section III.B.2. In fact, a slightly modified version of Eq. (12), which is used for nonlinear concentric PROs, is shown below.

$$
\dot{x}_{0,N,CP} = \frac{\|\vec{V}_r\|}{\|\vec{V}_{L,CP}\|}\dot{x}_{0,L,CP} + \left(\frac{\|\vec{V}_r\|}{\|\vec{V}_{L,CP}\|} - 1\right)(v_x - y_0\omega_z)
$$

$$
\dot{y}_{0,N,CP} = \frac{\|\vec{V}_r\|}{\|\vec{V}_{L,CP}\|}\dot{y}_{0,L,CP} + \left(\frac{\|\vec{V}_r\|}{\|\vec{V}_{L,CP}\|} - 1\right)\left(\frac{h}{r} + x_0\omega_z - z_0\omega_x\right) \tag{15}
$$

$$
\dot{z}_{0,N,CP} = \frac{\|\vec{V}_r\|}{\|\vec{V}_{L,CP}\|}\dot{z}_{0,L,CP} + \left(\frac{\|\vec{V}_r\|}{\|\vec{V}_{L,CP}\|} - 1\right)y_0\omega_x
$$

American Institute of Aeronautics and Astronautics

(a) First Orbit (b) Orbit Drift

Figure 6. The projection in the x-y plane of concentric PROs

where

$$\vec{V}_{L,CP} = (v_x + \dot{x}_{0,L,CP} - y_0\omega_z)\hat{x} + (\frac{h}{r} + \dot{y}_{0,L,CP} + x_0\omega_z - z_0\omega_x)\hat{y} + (\dot{z}_{0,L,CP} + y_0\omega_x)\hat{z} \qquad (16)$$

and $\|\vec{V}_r\|$ is defined in Eq. (9).

Then, using the conditions in Eq. (14), Eq. (15) results in the following equation.

$$
\begin{aligned}
\dot{x}_{0,N,CP} &= \frac{\|\vec{V}_r\|}{\|\vec{V}_{L,CP}\|}\left(\frac{1}{2}\omega_z y_0\right) + \left(\frac{\|\vec{V}_r\|}{\|\vec{V}_{L,CP}\|} - 1\right)(v_x - y_0\omega_z) \\
\dot{y}_{0,N,CP} &= \frac{\|\vec{V}_r\|}{\|\vec{V}_{L,CP}\|}\left(-2\omega_z x_0\right) + \left(\frac{\|\vec{V}_r\|}{\|\vec{V}_{L,CP}\|} - 1\right)\left(\frac{h}{r} + x_0\omega_z - z_0\omega_x\right) \\
\dot{z}_{0,N,CP} &= \left(\frac{\|\vec{V}_r\|}{\|\vec{V}_{L,CP}\|} - 1\right)y_0\omega_x
\end{aligned}
\qquad (17)
$$

Applying the initial conditions in Eq. (17) to the nominal swarm gives the results that are very similar to those seen in Fig. 5. As with period matching, the nonlinear conditions eliminate errors caused by linearization but does not dramatically improve the collision or drift behavior of the swarm under exact dynamics with J_2 only.

Although the concentric PROs method provides functional swarm motion for 60 orbits, it is not sufficient for a full mission. The amount of collisions occurring between orbit 60 and orbit 200 will definitely prevent the swarm from functioning; therefore, this approach will not work for any mission longer than a few days. In Section IV, initial conditions will be developed which provide collision free orbits for missions which last for months. Additionally, the PROs will drift at different rates depending on the orbital elements of the chief orbit. Therefore, this jump in the collision fraction can occur as early as the 10 orbit mark. The concentric PROs can provide desired trajectories for use in a feedback controller[21] but on its own it does not achieve good swarm keeping performance. Instead, the effects of the J_2 dynamics need to be taken into account when deriving initial conditions for collision free swarm keeping.

IV. Main Results: Swarm Keeping Methods for J_2 Perturbed Orbits

In the previous section, initial conditions were derived for collision free swarm motion using the Keplerian dynamics. The effectiveness of these conditions in a J_2 perturbed environment was tested by numerically integrating the exact dynamics with J_2 only. After making several adjustments to the initial conditions, it

American Institute of Aeronautics and Astronautics

was determined that the J_2 effect will cause spacecraft to collide and drift apart after a certain number of orbits. In this section, the initial conditions derived in Section III are modified to take into account the effects of J_2 on the swarm motion. Atmospheric drag will be discussed in Section V but it is neglected in this section because the accelerations due to J_2 are several orders of magnitude larger than those caused by drag. The J_2 perturbation affects relative motion in two ways: the crosstrack motion becomes coupled with the in-plane motion and the gravity gradient direction and magnitude are no longer constant.

A. Effects of Crosstrack Motion

In the HCW equations or Keplerian dynamics, the crosstrack, or out of plane motion, is uncoupled from the in plane motion. However, with the addition of the J_2 terms the motion becomes coupled in all three directions. This causes a growth in the crosstrack oscillation,[7] which will cause secular drift in the alongtrack direction if it is not accounted for. In order to eliminate this growth, we write the equation for the first order approximation of the crosstrack motion as follows.

$$z = r \sin \theta \delta i - r \cos \theta \sin i \delta \Omega \tag{18}$$

In this equation, δi and $\delta \Omega$ represent the differential inclination and right ascension, respectively. The only term in Eq. (18) that can have a secular drift is $\delta \Omega$ (see the equations of motion of the chief orbit in Appendix A) since r and i do not have secular terms due to J_2. Taking the derivative of $\delta \Omega$ results in

$$\delta \dot{\Omega} = \dot{\Omega}_j - \dot{\Omega} \tag{19}$$

where Ω_j is the right ascension of the deputy spacecraft. Substituting in for $\dot{\Omega}$ and $\dot{\Omega}_j$ using GVEs, integrating over an entire orbit to obtain the secular drift, setting the secular drift to zero, and simplifying yields

$$z(t) = B \cos \theta(t) = B \cos (\omega_z t + \theta_0) \tag{20}$$

where B is a constant and θ_0 is the initial argument of latitude of the chief spacecraft. This equation specifies that the crosstrack motion must have a certain phase with respect to the orbital motion in order to avoid growth in the amplitude of the crosstrack motion.

We also have the following equation for crosstrack motion from Eq (4).

$$z(t) = z_0 \cos \omega_z t + \frac{\dot{z}_0}{\omega_z} \sin \omega_z t \tag{21}$$

Equating Eq. (20) and Eq. (21), and applying the two conditions in Eq. (14) result in the following conditions.

$$\dot{x}_{0,L,J2} = \frac{1}{2} \omega_z y_0, \quad \dot{y}_{0,L,J2} = -2 \omega_z x_0, \quad \dot{z}_{0,L,J2} = -\omega_z z_0 \tan \theta_0 \tag{22}$$

The results of applying Eq. (22) are shown in Fig. 7. In Fig. 7a, the drift rate of the swarm is 15.5 m/orbit. This is a slight improvement over the period matched and concentric PRO swarms. Additionally, Fig. 7b shows that the collision fraction remains under 0.1 for the first 80 orbits and remains under 0.5 for the entire 500 orbit simulation. Additionally, the fuel required to perform this method is 1.55 m/s, which is about a 40% increase compared to a concentric PRO swarm. Once again, the drift and collision results are improved compared to the previous methods. However, these results must be improved further if the initial conditions are to provide collision free motion.

It is important to note that the third condition in Eq. (22) depends on $\tan \theta_0$ and therefore can potentially require an infinite velocity. For this reason, it is recommended that the burn be applied at the equator, if possible, in order to minimize the fuel used. Additionally, if the burn must be applied when $|\tan \theta_0| > 1$, we recommend using $|\tan \theta_0| = 1$ and then applying an additional burn once $|\tan \theta| \leq 1$. For, some applications, such as projected circular orbits (PCO), it is desired that the $y - z$ projection be a circle. In this case the required velocity in the crosstrack direction is fixed by the desired shape of the swarm. Therefore, we choose when to burn, or θ_0, so that we do not violate Eq. (22) and we still achieve a circular projection. In this example it is likely that the burn will be non equatorial.

American Institute of Aeronautics and Astronautics

(a) Drift results   (b) Collision results
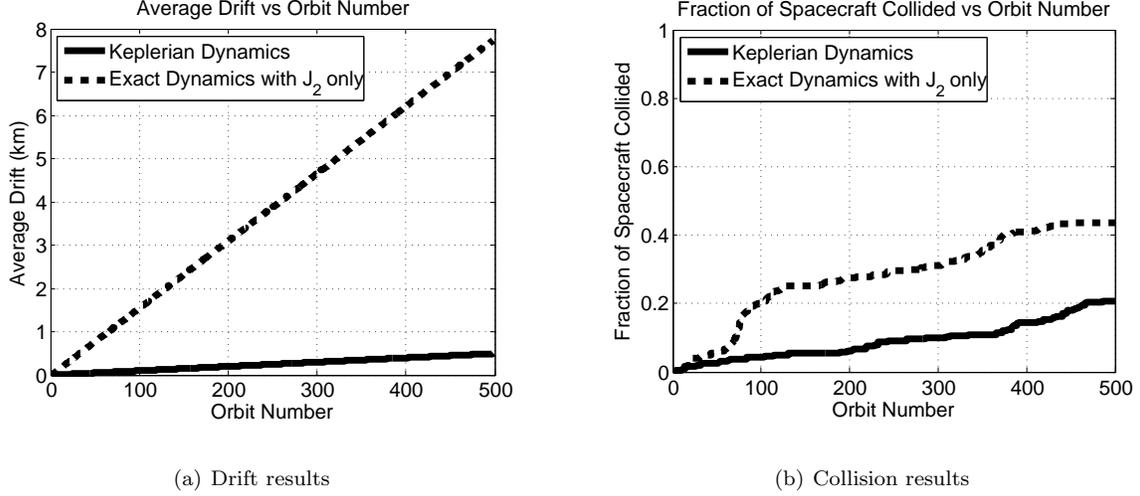
Figure 7. Simulation results of a linearized concentric PRO swarm with no crosstrack drift

B. Effects of Gravity Gradient on Swarm Motion

Another difference that arises with the addition of J_2 is the change in the gravity gradient vector caused by the J_2 disturbance. For a spherical Earth the gravity gradient vector has a constant direction and the magnitude depends only on r. The Keplerian gravity gradient vector is shown below.

$$\nabla U = \frac{\mu}{r^2}\hat{x} \tag{23}$$

The gradient of the gravitational potential under the influence of J_2 is[18]

$$\nabla U_{J2} = \frac{\mu}{r^2}\hat{x} + \frac{k_{J2}}{r^4}(1 - 3\sin^2 i \sin^2 \theta)\hat{x} + \frac{k_{J2}\sin^2 i \sin 2\theta}{r^4}\hat{y} + \frac{k_{J2}\sin 2i \sin \theta}{r^4}\hat{z} \tag{24}$$

Since ∇U_{J2} is not aligned with the radial direction, we define a new coordinate system $(\hat{x}'', \hat{y}'', \hat{z}'')$ so that $\hat{x}''$ is aligned with ∇U_{J2} and $\hat{y}''$ remains in the orbital plane. This new coordinate system is achieved by rotating the LVLH frame counterclockwise about the z axis by the angle α resulting in the intermediate coordinate system $(\hat{x}', \hat{y}', \hat{z}')$. Then, this coordinate system is rotated clockwise about the $\hat{y}'$ axis by an angle β to arrive at the desired coordinate system $(\hat{x}'', \hat{y}'', \hat{z}'')$. The angles α and β are functions of the chief's orbital parameters and are defined as follows:

$$\alpha = \arctan\left(\frac{\nabla U_{J2} \cdot \hat{y}}{\nabla U_{J2} \cdot \hat{x}}\right) \tag{25}$$

$$\beta = \arctan\left(\frac{\nabla U_{J2} \cdot \hat{z}}{\sqrt{(\nabla U_{J2} \cdot \hat{x})^2 + (\nabla U_{J2} \cdot \hat{y})^2}}\right) \tag{26}$$

Now that we have a coordinate system aligned with the gravitational potential gradient, we can apply Eq. (22) using the new coordinate system to get

$$\begin{bmatrix} \dot{x}''_{0,L,J2} \\ \dot{y}''_{0,L,J2} \\ \dot{z}''_{0,L,J2} \end{bmatrix} = \begin{bmatrix} 0 & \frac{1}{2}\omega''_z & 0 \\ -2\omega''_z & 0 & 0 \\ 0 & 0 & -\omega''_z \tan\theta_0 \end{bmatrix} \begin{bmatrix} x''_0 \\ y''_0 \\ z''_0 \end{bmatrix} \tag{27}$$

where the orbital angular rate ω''_z is

$$\omega''_z = \sqrt{\frac{\|\nabla U_{J2}\|}{r}} \tag{28}$$

Next, we need to transform Eq. (27) back into the LVLH coordinates. To do this we need the transformation equations for both rotations. The first and second rotation are described by Eq. (29) and Eq. (30), respectively.

$$
\begin{bmatrix} x' \\ y' \\ z' \end{bmatrix} = \begin{bmatrix} \cos\alpha & \sin\alpha & 0 \\ -\sin\alpha & \cos\alpha & 0 \\ 0 & 0 & 1 \end{bmatrix} \begin{bmatrix} x \\ y \\ z \end{bmatrix}
\tag{29}
$$

$$
\begin{bmatrix} x'' \\ y'' \\ z'' \end{bmatrix} = \begin{bmatrix} \cos\beta & 0 & \sin\beta \\ 0 & 1 & 0 \\ -\sin\beta & 0 & \cos\beta \end{bmatrix} \begin{bmatrix} x' \\ y' \\ z' \end{bmatrix}
\tag{30}
$$

Substituting Eq. (30) into the right hand side of Eq. (27) yields

$$
\begin{bmatrix} \dot{x}''_{0,L,J2} \\ \dot{y}''_{0,L,J2} \\ \dot{z}''_{0,L,J2} \end{bmatrix} = \begin{bmatrix} 0 & \frac{1}{2}\omega''_z & 0 \\ -2\omega''_z\cos\beta & 0 & -2\omega''_z\sin\beta \\ \omega''_z\sin\beta\tan\theta_0 & 0 & -\omega''_z\cos\beta\tan\theta_0 \end{bmatrix} \begin{bmatrix} x'_0 \\ y'_0 \\ z'_0 \end{bmatrix}
\tag{31}
$$

and substituting Eq. (29) into the right hand side of Eq. (31) gives

$$
\begin{bmatrix} \dot{x}''_{0,L,J2} \\ \dot{y}''_{0,L,J2} \\ \dot{z}''_{0,L,J2} \end{bmatrix} = \begin{bmatrix} -\frac{1}{2}\omega''_z\sin\alpha & \frac{1}{2}\omega''_z\cos\alpha & 0 \\ -2\omega''_z\cos\alpha\cos\beta & -2\omega''_z\sin\alpha\cos\beta & -2\omega''_z\sin\beta \\ \omega''_z\cos\alpha\sin\beta\tan\theta_0 & \omega''_z\sin\alpha\sin\beta\tan\theta_0 & -\omega''_z\cos\beta\tan\theta_0 \end{bmatrix} \begin{bmatrix} x_0 \\ y_0 \\ z_0 \end{bmatrix}
\tag{32}
$$

Now solve for $(\dot{x}_{0,L}, \dot{y}_{0,L}, \dot{z}_{0,L})$ in terms of $(\dot{x}''_{0,L}, \dot{y}''_{0,L}, \dot{z}''_{0,L})$ by inverting Eq. (29) and substituting in the inverse of Eq. (30).

$$
\begin{bmatrix} \dot{x}_{0,L,J2} \\ \dot{y}_{0,L,J2} \\ \dot{z}_{0,L,J2} \end{bmatrix} = \begin{bmatrix} \cos\alpha\cos\beta & -\sin\alpha & -\cos\alpha\sin\beta \\ \sin\alpha\cos\beta & \cos\alpha & -\sin\alpha\sin\beta \\ \sin\beta & 0 & \cos\beta \end{bmatrix} \begin{bmatrix} \dot{x}''_{0,L,J2} \\ \dot{y}''_{0,L,J2} \\ \dot{z}''_{0,L,J2} \end{bmatrix}
\tag{33}
$$

Finally, substituting Eq. (32) into the right hand side of Eq. (33) results in the desired initial conditions shown below.

$$
\begin{bmatrix} \dot{x}_{0,L,J2} \\ \dot{y}_{0,L,J2} \\ \dot{z}_{0,L,J2} \end{bmatrix} = \omega''_z \begin{bmatrix} \frac{3}{2}c_\alpha s_\alpha c_\beta - c_\alpha^2 s_\beta^2 t_{\theta_0} & \frac{1}{2}c_\alpha^2 c_\beta + 2s_\alpha^2 c_\beta - c_\alpha s_\alpha s_\beta^2 t_{\theta_0} & 2s_\alpha s_\beta + c_\alpha c_\beta s_\beta t_{\theta_0} \\ -2c_\alpha^2 c_\beta - \frac{1}{2}s_\alpha^2 c_\beta - c_\alpha s_\alpha s_\beta^2 t_{\theta_0} & -\frac{3}{2}c_\alpha s_\alpha c_\beta - s_\alpha^2 s_\beta^2 t_{\theta_0} & -2c_\alpha s_\beta + s_\alpha c_\beta s_\beta t_{\theta_0} \\ -\frac{1}{2}s_\alpha s_\beta + c_\alpha c_\beta s_\beta t_{\theta_0} & \frac{1}{2}c_\alpha s_\beta + s_\alpha c_\beta s_\beta t_{\theta_0} & -c_\beta^2 t_{\theta_0} \end{bmatrix} \begin{bmatrix} x_0 \\ y_0 \\ z_0 \end{bmatrix}
\tag{34}
$$

where $s_{(\cdot)}$, $c_{(\cdot)}$, and $t_{(\cdot)}$ represent $\sin(\cdot)$, $\cos(\cdot)$, and $\tan(\cdot)$, respectively. These initial conditions are applied to the nominal swarm and the results are shown in Fig. 8.

Figure 8a shows the drift results for a nominal swarm. After 500 orbits, the swarm drifts by 2.6 m/orbit under the influence of J_2. This is a significant improvement over previous methods. However, the collision results of the J_2 adjusted swarm, shown in Fig. 8b, show that the collision fraction remains under 0.1 for 100 orbits but eventually reaches 0.75, which is not acceptable for a functioning swarm. The fuel usage is 1.55 m/s which is similar to the method in Section IV.A. These results show that the J_2 adjusted method is still not sufficient for collision free motion.

C. Energy Matching with J_2

The initial conditions from Eq. (34) greatly decrease the drift rate of the swarm by accounting for the change in magnitude and direction of the gravity gradient vector caused by the J_2 effect. The major problem with these equations is that they use Eq. (22) as a starting point. Therefore, these J_2 adjusted conditions assume a circular chief orbit and they are linearized. In order to eliminate these potential sources of error, a new set of initial conditions are derived using nonlinear energy matching instead of using the HCW equations to eliminate drift.

(a) Drift results

(b) Collision results
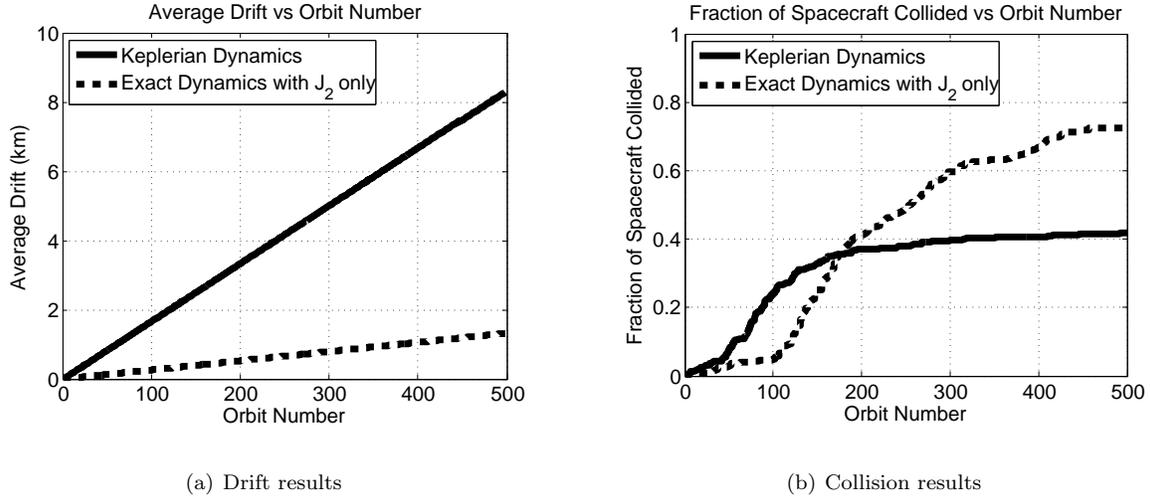
Figure 8. Simulation results of a swarm accounting for linearized J_2 effects

In order to ensure that the spacecraft do not drift apart, we match the total energy of each deputy spacecraft to the energy of the chief spacecraft. In the following energy matching condition, $\|\vec{V}_r\|$ is defined in Eq. (9) and $\vec{V}$ is defined in Eq. (6).

$$\frac{\|\vec{V}\|^2}{2} + U = \frac{\|\vec{V}_{r,J2}\|^2}{2} + U_j \tag{35}$$

where U and U_j are defined below.

$$U = -\frac{\mu}{r} - \frac{k_{J2}}{r^3}\left(\frac{1}{3} - \sin^2 i \sin^2 \theta\right) \tag{36}$$

$$U_j = -\frac{\mu}{r_j} - \frac{k_{J2}}{r_j^3}\left(\frac{1}{3} - \frac{r_{jZ}^2}{r_j^2}\right) \tag{37}$$

Equation (35) can be rewritten as

$$\|\vec{V}_{r,J2}\| = \sqrt{\|\vec{V}\|^2 + 2(U - U_j)} \tag{38}$$

Now that we have established the desired velocity for an energy matched spacecraft in the presence of J_2, we can use the modified version of Eq. (12) shown below

$$\dot{x}_{0,N,J2} = \frac{\|\vec{V}_{r,J2}\|}{\|\vec{V}_{L,J2}\|}\dot{x}_{0,L,J2} + \left(\frac{\|\vec{V}_{r,J2}\|}{\|\vec{V}_{L,J2}\|} - 1\right)(v_x - y_0\omega_z)$$

$$\dot{y}_{0,N,J2} = \frac{\|\vec{V}_{r,J2}\|}{\|\vec{V}_{L,J2}\|}\dot{y}_{0,L,J2} + \left(\frac{\|\vec{V}_{r,J2}\|}{\|\vec{V}_{L,J2}\|} - 1\right)\left(\frac{h}{r} + x_0\omega_z - z_0\omega_x\right) \tag{39}$$

$$\dot{z}_{0,N,J2} = \frac{\|\vec{V}_{r,J2}\|}{\|\vec{V}_{L,J2}\|}\dot{z}_{0,L,J2} + \left(\frac{\|\vec{V}_{r,J2}\|}{\|\vec{V}_{L,J2}\|} - 1\right)y_0\omega_x$$

where

$$\vec{V}_{L,J2} = (v_x + \dot{x}_{0,L,J2} - y_0\omega_z)\hat{x} + (\frac{h}{r} + \dot{y}_{0,L,J2} + x_0\omega_z - z_0\omega_x)\hat{y} + (\dot{z}_{0,L,J2} + y_0\omega_x)\hat{z} \tag{40}$$

Then, applying the conditions in Eq. (34) to Eq. (39) results in the main J_2 invariant swarm keeping equations. The following J_2 invariant equations use energy matching to build upon the results from Eq. (22) and Eq. (34).

American Institute of Aeronautics and Astronautics

$$\dot{x}_{0,N,J2} = \frac{\|\vec{V}_{r,J2}\|}{\|\vec{V}_{L,J2}\|} \left[\left(\frac{3}{2} c_\alpha s_\alpha c_\beta - c_\alpha^2 s_\beta^2 t_{\theta_0} \right) x_0 + \left(\frac{1}{2} c_\alpha^2 c_\beta + 2 s_\alpha^2 c_\beta - c_\alpha s_\alpha s_\beta^2 t_{\theta_0} \right) y_0 + \left(2 s_\alpha s_\beta + c_\alpha c_\beta s_\beta t_{\theta_0} \right) z_0 \right] \omega_z''$$

$$+ \left(\frac{\|\vec{V}_{r,J2}\|}{\|\vec{V}_{L,J2}\|} - 1 \right) (v_x - y_0 \omega_z)$$

$$\dot{y}_{0,N,J2} = \frac{\|\vec{V}_{r,J2}\|}{\|\vec{V}_{L,J2}\|} \left[\left(-2 c_\alpha^2 c_\beta - \frac{1}{2} s_\alpha^2 c_\beta - c_\alpha s_\alpha s_\beta^2 t_{\theta_0} \right) x_0 + \left(-\frac{3}{2} c_\alpha s_\alpha c_\beta - s_\alpha^2 s_\beta^2 t_{\theta_0} \right) y_0 + \left(-2 c_\alpha s_\beta + s_\alpha c_\beta s_\beta t_{\theta_0} \right) z_0 \right] \omega_z''$$

(41)

$$+ \left(\frac{\|\vec{V}_{r,J2}\|}{\|\vec{V}_{L,J2}\|} - 1 \right) \left(\frac{h}{r} + x_0 \omega_z - z_0 \omega_x \right)$$

$$\dot{z}_{0,N,J2} = \frac{\|\vec{V}_{r,J2}\|}{\|\vec{V}_{L,J2}\|} \left[\left(-\frac{1}{2} s_\alpha s_\beta + c_\alpha c_\beta s_\beta t_{\theta_0} \right) x_0 + \left(\frac{1}{2} c_\alpha s_\beta + s_\alpha c_\beta s_\beta t_{\theta_0} \right) y_0 + \left(-c_\beta^2 t_{\theta_0} \right) z_0 \right] \omega_z''$$

$$+ \left(\frac{\|\vec{V}_{r,J2}\|}{\|\vec{V}_{L,J2}\|} - 1 \right) y_0 \omega_x$$

where α and β are defined in Eq. (25) and Eq. (26), respectively. Additionally, $s_{(\cdot)}, c_{(\cdot)}$, and $t_{(\cdot)}$ represent $\sin(\cdot)$, $\cos(\cdot)$, and $\tan(\cdot)$, respectively.

(a) Drift results   (b) Collision results
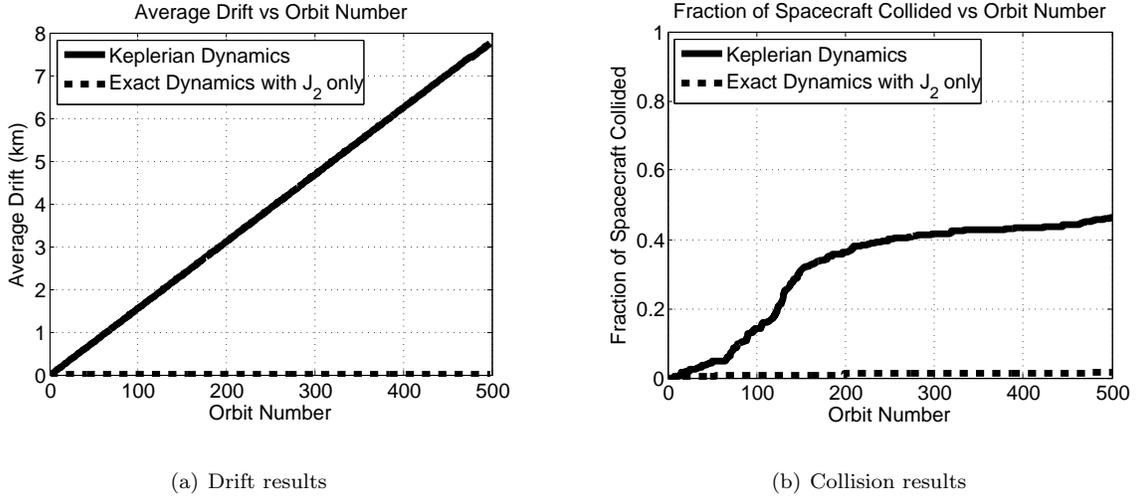
Figure 9. Simulation results of an energy matched swarm

The energy matching conditions in Eq. (41) show a significant improvement in collision and drift results compared to the linearized conditions. This is because the drift due to J_2 has been significantly reduced so that the errors due to linearization and eccentricity are dominant. Therefore, eliminating these errors by using the nonlinear conditions has a huge impact on the performance of the swarm and the drift rate in Fig. 9a is 7.55 mm/orbit, which is about three orders of magnitude better than any other methods. Additionally, Fig. 9b shows that the collision fraction remains under 2% for 500 orbits. Additionally, the fuel usage is about 1.55 m/s, which is comparable to the previous methods. Therefore, the energy matched conditions prevent collisions for more than 500 orbits while still using only a single burn of similar magnitude to the other methods.

The results of the energy matched swarm for various altitudes, eccentricities, and inclinations are displayed in Tables 1-3, respectively. After 500 orbits, at least 39% of the nonlinear concentric PRO swarm has collided in all of the simulations run. However, in all of the energy matched swarms, less than 2% of the swarm has collided. It is important to note that 2% is only five collisions and these collisions are probably caused by the fact that the spacecraft are simply located too close together initially. In the following subsec-

tion, we will derive a condition for the initial separation between any two spacecraft which guarantees that collisions do not occur because of poor initial spacing in the swarm.

Table 1. Drift rate and collision fraction after 500 orbits for nonlinear concentric PRO and energy matched swarms with varying altitude, 0 eccentricity, 45 degree inclination, and 45 degree argument of latitude

	Concentric PRO (Eq. (17))		J_2 Energy Matched (Eq. (41))	
Altitude [km]	Drift Rate [m/orbit]	Collisions [%]	Drift Rate [m/orbit]	Collisions [%]
300	21.65	55.4	0.00851	1.2
500	20.41	58.0	0.00755	1.6
800	18.73	54.2	0.00636	1.2
1000	17.73	56.6	0.00570	0.8

Table 2. Drift rate and collision fraction after 500 orbits for nonlinear concentric PRO and energy matched swarms with 500 km altitude, varying eccentricity, 45 degree inclination, and 45 degree argument of latitude

	Concentric PRO (Eq. (17))		J_2 Energy Matched (Eq. (41))	
Eccentricity	Drift Rate [m/orbit]	Collisions [%]	Drift Rate [m/orbit]	Collisions [%]
0	20.41	58.0	0.00755	1.6
0.001	20.45	51.4	0.00765	1.2
0.01	20.82	41.8	0.03292	0.8

Table 3. Drift rate and collision fraction after 500 orbits for nonlinear concentric PRO and energy matched swarms with 500 km altitude, 0 eccentricity, varying inclination, and 45 degree argument of latitude

	Concentric PRO (Eq. (17))		J_2 Energy Matched (Eq. (41))	
Inclination [degrees]	Drift Rate [m/orbit]	Collisions [%]	Drift Rate [m/orbit]	Collisions [%]
0	10.70	39.0	0.02010	0.4
30	18.12	45.4	0.00954	0.8
45	20.41	58.0	0.00755	1.6
60	19.00	48.2	0.00478	0.8
90	11.25	47.8	0.00581	0.4

D.   Collision Free Conditions

The energy matching conditions in Eq. (41) ensure that the relative orbits of the spacecraft do not drift enough to cause collisions for over 500 orbits. However, this alone does not guarantee collision free motion of the swarm. The initial position of each spacecraft must also satisfy a condition to make sure that no collisions occur within the first orbit. In order to check for collisions within the first orbit, we make the assumption that each spacecraft is on a concentric PRO. This assumption is accurate because the J_2 drift is minimal due to both the energy matching conditions and the small time frame (only the first orbit) being considered.

Proposition 1:   If two spacecraft are on concentric PROs under the HCW equations, then a sufficient condition for collision free motion is that their initial positions satisfy[20]

$$\sqrt{\delta x_0^2 + \delta y_0^2} > 2X \tag{42}$$

where $\sqrt{\delta x_0^2 + \delta y_0^2}$ is the initial projected distance between two spacecraft and X is the minimum distance at which two spacecraft will collide. This condition ensures that two spacecraft will never come within a distance X of each other for all time.

American Institute of Aeronautics and Astronautics

Proposition 1 is proved rigorously in Acikmese *et al.*[20] under the HCW equations. However, it is useful to invoke here as a heuristic to ensure that there are no poor initial conditions when initializing a swarm with respect to Keplerian or exact relative dynamics. Combining the condition in Eq. (42) with the J_2 energy matched conditions in Eq. (41) provides collision free motion. Depending on the length of the mission, we can choose the relative semi-major axis and phase of each spacecraft so that they will not collide for the duration of the mission. This can be done by calculating the worst case drift and placing the spacecraft on PROs whose semi-major axes differ by more than the worst case drift. This will ensure that the PROs never drift far enough to intersect with another PRO and therefore no collisions will occur.

V.   Swarm Keeping for J_2 and Atmospheric Drag Perturbed Orbits

This section shows the effects of atmospheric drag on energy matched swarms. Although atmospheric drag effects are several orders of magnitude smaller than J_2 effects, atmospheric drag is a non-conservative force, which means that energy matching the spacecraft cannot be used to account for atmospheric drag effects. In order to account for atmospheric drag, we develop a multi-burn guidance method, which adjusts the states of each spacecraft every orbit in order to maintain collision free motion.

A.   Atmospheric Drag

The conditions developed in Eq. (41) have been shown to eliminate collisions for spacecraft swarms in the presence of J_2. In this section, we look into the effects of atmospheric drag on an energy matched swarm. In order to do this, the energy matching conditions are applied to the swarm but this time atmospheric drag is included in the simulation. The collision and drift results from this simulation are shown in Fig. 10.

(a) Drift results

(b) Collision results
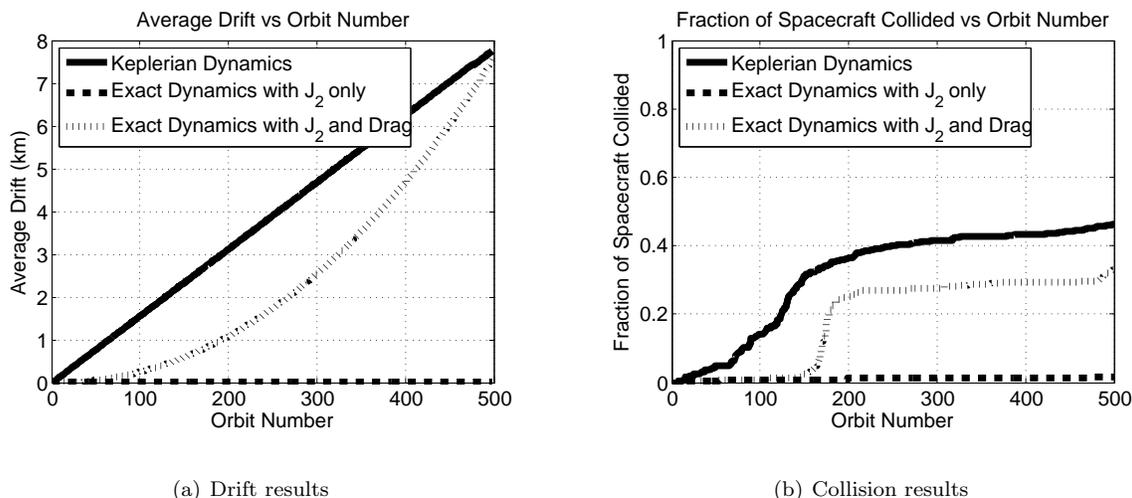
Figure 10. Simulation results of an energy matched swarm under the influence of J_2 and atmospheric drag

Figure 10 shows that the addition of atmospheric drag causes the swarm to disperse which then causes the spacecraft to collide after only 100 orbits. Therefore, the energy matching conditions do not prevent collisions when atmospheric drag is significant. Since atmospheric drag is dependent on many factors including spacecraft mass, cross-sectional area, and altitude, there may be certain missions where the effect of atmospheric drag is so small that the energy matching conditions provide collision free motion. For this simulation, the values of the cross sectional area (A) and mass (m) of the spacecraft were chosen to be 0.01 [m^2] and 0.1 [kg], respectively. These are very conservative values and it is likely that the cross sectional area of the spacecraft is smaller and that the mass is larger than the values used in these simulations. Both of these changes will decrease the effect of atmospheric drag on the motion of the swarm.

It is important to note that this simulation is run assuming that all of the spacecraft have the same physical properties. Therefore, the virtual chief spacecraft takes on the same physical characteristics as the other spacecraft. However, if there is a heterogeneous swarm, spacecraft have different shapes or masses, the

choice of the chief's physical parameters is arbitrary. The motion of the deputies relative to each other will not depend on the physical parameters of the chief. However, the entire swarm will move with respect to the chief orbit if the chief's physical parameters are chosen poorly. For this reason, it is suggested that chief's parameters be equal to the average of the deputies so that the chief orbit remains within the swarm. In all of the simulations run in this paper, each spacecraft is modeled as a sphere so that C_d is not dependent on the orientation of each spacecraft.

B.   Multi-Burn Guidance Method

In order to eliminate the effects of atmospheric drag on the swarm, a multi-burn guidance method is proposed in this section. This controller uses the energy matching initial conditions but rather than burning only once at the beginning of the mission, this method uses multiple burns to correct for the drift caused by atmospheric drag. Depending on the available fuel and swarm drift allotted by the mission, these corrections can be made at various frequencies ranging from multiple times per orbit to once every hundred orbits. However, the energy matching conditions are much more efficient at the equator than they are near the poles. Therefore, it is recommended that burns occur only when $\theta = k \times \pi$ where k is a nonnegative integer. This results in zero crosstrack velocity, which reduces the amount of fuel required to perform the manuever. The multi-burn guidance method using one burn per orbit is illustrated in Fig. 11
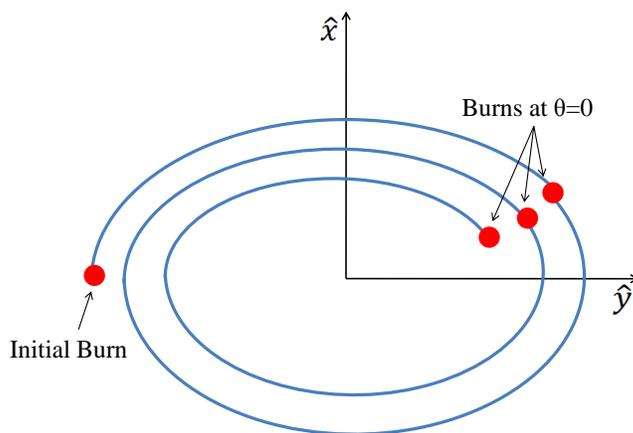
Figure 11.   Illustration of the multi-burn guidance method in the LVLH frame

Figure 12 clearly shows that applying the energy matching initial conditions from Eq. (41) once per orbit reduces the drift caused by atmospheric drag and provides collision free motion for over 500 orbits. This multi-burn guidance method maintains the size of the swarm and prevents collisions within the swarm uin the presence the the two major perturbations in LEO, J_2 effects and atmospheric drag. In the simulation shown in Fig. 12, the first burn occur at $\theta = 45$ degrees because that is the initial position but all subsequent burns occur at $\theta = 0$ degrees in order to minimize fuel.

The multi-burn guidance method can be applied regardless of the initial argument of latitude. If there is no desired swarm shape, the first burn should occur immediately, regardless of the initial argument of latitude, and the following burns should occur at the equator in order to minimize fuel. However, it may be desirable to maintain a specific swarm shape, such as a projected circular orbit. In this case it may not be possible to achieve this shape and burn at the equator. Therefore, based on the desired crosstrack velocity, the argument of latitude at which the burn must occur can be calculated based on Eq. (22). In this scenario, the first burn should occur immediately and the following burns should occur at the argument of latitude which produces the desired crosstrack motion. This method minimizes fuel usage and drift while still permitting a variety of swarm shapes.

(a) Drift results   (b) Collision results
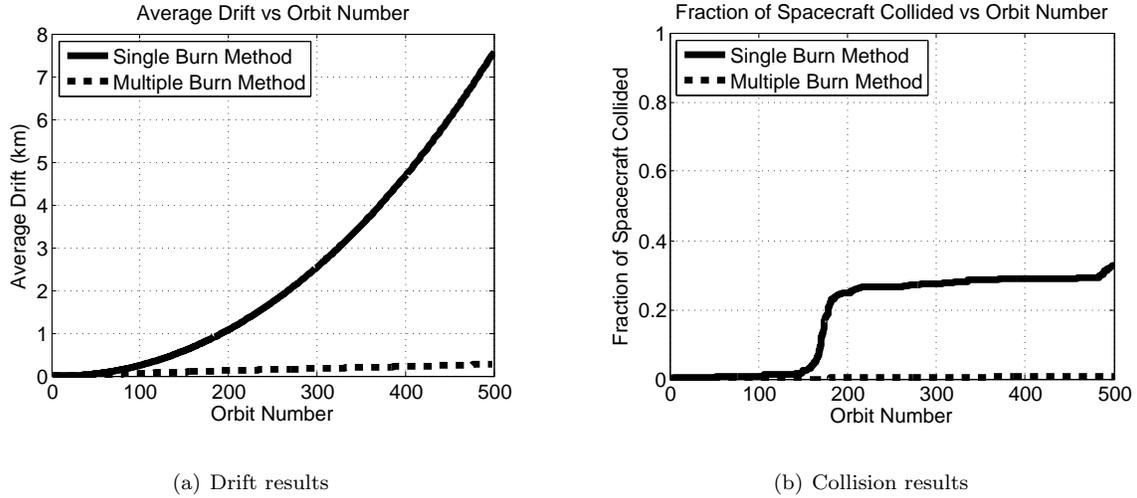
Figure 12. Simulation results of the multiburn guidance method under the influence of J_2 and atmospheric drag

VI.   Conclusion

In this paper, we explored the swarm keeping problem for a swarm of hundreds of spacecraft. We introduced the notion of swarm keeping as maintaining relative distances between multiple spacecraft in the presence of disturbances and ensuring that collisions do not occur. The number of spacecraft along with their modest capabilities provided new challenges which have not been addressed in previous studies. The large number of spacecraft makes online path planning or reactive collision avoidance extremely difficult. Therefore, we developed a set of initial conditions that provide collision free motion for hundreds of orbits in the presence of J_2 perturbations. Furthermore, such initial conditions coincide with a fuel-efficient strategy since very little fuel is required to stay on J_2 invariant relative orbits.

The main results developed in Section IV establish J_2 invariant relative orbits by applying the energy matching method after correcting for the effects of the gravity gradients and J_2-perturbed cross-track motions. The proposed swarm keeping initial conditions were shown by computer simulation to greatly reduce both the swarm drift rate and the collision rate across a wide range of reference orbits regardless of altitude, eccentricity, and inclination (e.g., a drift rate of 7.55 mm/orbit and a collision fraction of 1.6% for the reference orbit of 500 km, 0 eccentricity, and 45 deg inclination).

The performance of collision free motions can deteriorate over time in the presence of air drag especially in lower LEO. Another contribution of the paper lies in deriving a new set of nonlinear dynamics which include both J_2 effects and atmospheric drag. This new dynamic model was used to test the energy matching conditions in the presence of atmospheric drag. Finally, a multi-burn guidance method, which sequentially employs the main initial conditions of J_2 invariant relative orbits, was developed to correct for the effects of atmospheric drag. This controller was shown by computer simulation to provide collision free motion over hundreds of orbits for spacecraft swarms in the presence of the two dominant disturbances in LEO, J_2 and atmospheric drag.

Appendix A: Exact Dynamics of Reference Orbit with J_2 and Drag

Proposition 2:   Considering the two main disturbances in LEO, J_2 gravity and atmospheric drag, the differential equations describing the motion of the chief orbit are as follows:

American Institute of Aeronautics and Astronautics

$$\dot{r} = v_x \tag{43}$$

$$\dot{v}_x = -\frac{\mu}{r^2} + \frac{h^2}{r^3} - \frac{k_{J2}}{r^4}(1 - 3\sin^2 i \sin^2 \theta) - C\|\vec{V}_a\|v_x \tag{44}$$

$$\dot{h} = -\frac{k_{J2}\sin^2 i \sin 2\theta}{r^3} - C\|\vec{V}_a\|(h - \omega_e r^2 \cos i) \tag{45}$$

$$\dot{\Omega} = -\frac{2k_{J2}\cos i \sin^2 \theta}{hr^3} - \frac{C\|\vec{V}_a\|\omega_e r^2 \sin 2\theta}{2h} \tag{46}$$

$$\dot{i} = -\frac{k_{J2}\sin 2i \sin 2\theta}{2hr^3} - \frac{C\|\vec{V}_a\|\omega_e r^2 \sin i \cos^2 \theta}{h} \tag{47}$$

$$\dot{\theta} = \frac{h}{r^2} + \frac{2k_{J2}\cos^2 i \sin^2 \theta}{hr^3} + \frac{C\|\vec{V}_a\|\omega_e r^2 \cos i \sin 2\theta}{2h} \tag{48}$$

Proof: The rotation rate of the LVLH frame[22] is composed of the following components:

$$\omega_x = \dot{i}\cos\theta + \dot{\Omega}\sin\theta\sin i \tag{49}$$

$$\omega_y = -\dot{i}\sin\theta + \dot{\Omega}\cos\theta\sin i = 0 \tag{50}$$

$$\omega_z = \dot{\theta} + \dot{\Omega}\cos i = \frac{h}{r^2} \tag{51}$$

The motion of the chief spacecraft is determined by the following equation:

$$\ddot{\vec{r}} = -\nabla U_{J2} + \vec{a}_{drag} \tag{52}$$

where the gradient of the J_2 perturbed gravitational potential energy (∇U_{J2}) is defined in Eq. (24) The acceleration due to drag is

$$\vec{a}_{drag} = -\frac{1}{2}C_d\frac{A}{m}\rho\|\vec{V}_a\|\vec{V}_a \tag{53}$$

In order to simplify the drag expression, we define a new constant $C = \frac{1}{2}C_d\frac{A}{m}\rho$. The velocity of the chief spacecraft with respect to the atmosphere is found from the following equation.

$$\vec{V}_a = \vec{V} - \vec{\omega}_e \times \vec{r} \tag{54}$$

where

$$\vec{V} = v_x\hat{x} + \frac{h}{r}\hat{y}$$
$$\vec{r} = r\hat{x} \tag{55}$$
$$\vec{\omega}_e = \omega_e\hat{Z} = \omega_e(\sin\theta\sin i\hat{x} + \cos\theta\sin i\hat{y} + \cos i\hat{z})$$

Evaluating Eq. (54) yields

$$\vec{V}_a = v_x\hat{x} + \left(\frac{h}{r} - \omega_e r \cos i\right)\hat{y} + \omega_e r \cos\theta\sin i\hat{z} \tag{56}$$

where $\omega_e = 7.2921 \times 10^{-5}$ [rad/s]. Taking the second derivative of $\vec{r}$ yields

$$\ddot{\vec{r}} = \left(\dot{v}_x - \frac{h^2}{r^3}\right)\hat{x} + \frac{\dot{h}}{r}\hat{y} + \frac{\omega_x h}{r}\hat{z} \tag{57}$$

where we define $v_x = \dot{r}$ establishing Eq. (43). Evaluating the right hand side of Eq. (52) yields

American Institute of Aeronautics and Astronautics

$$-\nabla U_{J2} + \vec{a}_{drag} = -\left[\frac{\mu}{r^2} + \frac{k_{J2}}{r^4}(1 - 3\sin^2 i \sin^2 \theta) + C\|\vec{V}_a\|v_x\right]\hat{x} - \left[\frac{k_{J2}\sin^2 i \sin 2\theta}{r^4} + C\|\vec{V}_a\|\left(\frac{h}{r} - \omega_e r \cos i\right)\right]\hat{y}$$

$$(58)$$

$$-\left[\frac{k_{J2}\sin 2i \sin \theta}{r^4} + C\|\vec{V}_a\|\omega_e r \cos \theta \sin i\right]\hat{z}$$

Substituting Eq. (57) and Eq. (58) into Eq. (52) establishes Eq. (44) and Eq. (45). Additionally, the following equation for the radial rotation rate of the coordinate system is developed.

$$\omega_x = -\frac{k_{J2}\sin 2i \sin \theta}{hr^3} - \frac{C\|\vec{V}_a\|\omega_e r^2 \cos \theta \sin i}{h} \tag{59}$$

Finally, we can solve Eqs. (49)-(51) and Eq. (59) in order to verify Eqs. (46)-(48). $\qquad\square$

Appendix B: Exact Relative Dynamics with J_2 and Drag

Proposition 3: Considering the J_2 perturbation and atmospheric drag, the relative equations of motion for the j-th spacecraft are shown below.

$$
\begin{aligned}
\ddot{x}_j =\,& 2\dot{y}_j\omega_z - x_j(\eta_j^2 - \omega_z^2) + y_j\alpha_z - z_j\omega_x\omega_z - (\zeta_j - \zeta)\sin i \sin \theta - r(\eta_j^2 - \eta^2) \\
& - C_j\|\vec{V}_{aj}\|(\dot{x}_j - y_j\omega_z) - (C_j\|\vec{V}_{aj}\| - C\|\vec{V}_a\|)v_x \\
\ddot{y}_j =\,& -2\dot{x}_j\omega_z + 2\dot{z}_j\omega_x - x_j\alpha_z - y_j(\eta_j^2 - \omega_z^2 - \omega_x^2) + z_j\alpha_x - (\zeta_j - \zeta)\sin i \cos \theta \\
& - C_j\|\vec{V}_{aj}\|(\dot{y}_j + x_j\omega_z - z_j\omega_x) - (C_j\|\vec{V}_{aj}\| - C\|\vec{V}_a\|)\left(\frac{h}{r} - \omega_e r \cos i\right) \\
\ddot{z}_j =\,& -2\dot{y}_j\omega_x - x_j\omega_x\omega_z - y_j\alpha_x - z_j(\eta_j^2 - \omega_x^2) - (\zeta_j - \zeta)\cos i \\
& - C_j\|\vec{V}_{aj}\|(\dot{z}_j + y_j\omega_x) - (C_j\|\vec{V}_{aj}\| - C\|\vec{V}_a\|)\omega_e r \cos \theta \sin i
\end{aligned}
\tag{60}
$$

where $\eta, \eta_j, \zeta, \zeta_j, r_j$, and r_{jZ} have been introduced in order to simplify the potential energy terms. There definitions are shown below.[18]

$$
\begin{aligned}
\zeta &= \frac{2k_{J2}\sin i \sin \theta}{r^4} \\
\zeta_j &= \frac{2k_{J2}r_{jZ}}{r^5} \\
\eta^2 &= \frac{\mu}{r^3} + \frac{k_{J2}}{r^5} - \frac{5k_{J2}\sin^2 i \sin^2 \theta}{r^5} \\
\eta_j^2 &= \frac{\mu}{r_j^3} + \frac{k_{J2}}{r_j^5} - \frac{5k_{J2}r_{jZ}^2}{r_j^5} \\
r_j &= \sqrt{(r + x_j)^2 + y_j^2 + z_j^2} \\
r_{jZ} &= (r + x_j)\sin i \sin \theta + y_j \sin i \cos \theta + z_j \cos i
\end{aligned}
\tag{61}
$$

Additionally, C_j is defined similarly to C except C_j uses the deputy values as shown below.

$$C_j = \frac{1}{2}C_{d,j}\frac{A_j}{m_j}\rho_j \tag{62}$$

The value of C_j corresponds to the j-th deputy spacecraft and each deputy will have a different value for C_j. In general, the drag coefficient ($C_{d,j}$), the cross sectional area (A_j), and the mass (m_j) can be different for each spacecraft but we assume that all spacecraft are the same shape and mass in our simulations for simplicity.

Proof: We start by finding the Lagrangian ($\mathcal{L}_j$) and substituting it into Lagrange's equation, which is shown below.

$$\frac{d}{dt}\left(\frac{\partial \mathcal{L}_j}{\partial \dot{q}_n}\right) - \frac{\partial \mathcal{L}_j}{\partial q_n} = Q_n \tag{63}$$

In this case, the q_n's are x_j, y_j, and z_j. Now we must find the Lagrangian ($\mathcal{L}_j = T_j - U_j$), which is the difference between kinetic and potential energy, and the generalized relative force in each direction (Q_n). The kinetic energy (per unit mass) can be found from

$$T_j = \frac{1}{2}\vec{V}_j \cdot \vec{V}_j = \frac{1}{2}[(v_x + \dot{x}_j - y_j\omega_z)^2 + (\frac{h}{r} + \dot{y}_j + x_j\omega_z - z_j\omega_x)^2 + (\dot{z}_j + y_j\omega_x)^2] \tag{64}$$

where $\vec{V}_j$ is the velocity of the deputy spacecraft and can be found from

$$\vec{V}_j = (v_x + \dot{x}_j - y_j\omega_z)\hat{x} + (\frac{h}{r} + \dot{y}_j + x_j\omega_z - z_j\omega_x)\hat{y} + (\dot{z}_j + y_j\omega_x)\hat{z} \tag{65}$$

The potential energy for the deputy spacecraft[18] (U_j) is defined in Eq. (37). Now we evaluate the Lagrangian.

$$\mathcal{L}_j = \frac{1}{2}[(v_x + \dot{x}_j - y_j\omega_z)^2 + (\frac{h}{r} + \dot{y}_j + x_j\omega_z - z_j\omega_x)^2 + (\dot{z}_j + y_j\omega_x)^2] + \frac{\mu}{r_j} + \frac{k_{J2}}{r_j^3}\left(\frac{1}{3} - \frac{r_{jZ}^2}{r_j^2}\right) \tag{66}$$

Substituting Eq. (66) into Eq. (63) yields the exact relative dynamics for spacecraft under the influence of J_2.[18] In order to derive a better dynamic model for spacecraft in LEO, we take into account the effect of atmospheric drag on the relative motion. By including both J_2 effects and drag, the dynamics derived in this paper include both of the major perturbations experienced by spacecraft in LEO and provide more accurate simulation results than any previous models.

Since the drag is a non-conservative force it must be found in the Q_n terms. The generalized forces will be the components of differential drag vector which is defined below.

$$\vec{F}_{\text{diff}} = \vec{F}_j - \vec{F} = -C_j\|\vec{V}_{aj}\|\vec{V}_{aj} + C\|\vec{V}_a\|\vec{V}_a \tag{67}$$

where C_j is defined in Eq. (62) and the velocity of the deputy with respect to the atmosphere is defined below.

$$\vec{V}_{aj} = \vec{V}_a + \dot{\vec{l}}_j + \vec{\omega} \times \vec{l}_j \tag{68}$$

where $\vec{l}_j$ is the relative position vector and $\dot{\vec{l}}_j$ is the relative velocity vector. The generalized forces can be obtained from Eq. (67) as follows.

$$Q_x = -C_j\|\vec{V}_{aj}\|(\dot{x}_j - y_j\omega_z) - (C_j\|\vec{V}_{aj}\| - C\|\vec{V}_a\|)v_x \tag{69}$$

$$Q_y = -C_j\|\vec{V}_{aj}\|(\dot{y}_j + x_j\omega_z - z_j\omega_x) - (C_j\|\vec{V}_{aj}\| - C\|\vec{V}_a\|)\left(\frac{h}{r} - \omega_e r\cos i\right) \tag{70}$$

$$Q_z = -C_j\|\vec{V}_{aj}\|(\dot{z}_j + y_j\omega_x) - (C_j\|\vec{V}_{aj}\| - C\|\vec{V}_a\|)\omega_e r\cos\theta\sin i \tag{71}$$

Now all of the values required for the Lagrangian equations of motion have been found. Substituting Eq. (66), Eq. (69), Eq. (70), and Eq. (71) into Eq. (63) results in the Lagrangian equations of motion. After much simplification, Eq. (60) is established. $\square$

Acknowledgments

References

[1] Aung, M., Ahmed, A., Wette, M., Scharf, D., Tien, J., Purcell, G., Regehr, M., and Landin, B., "An Overview of Formation Flying Technology Development for the Terrestrial Planet Finder Mission," *Proceedings of the IEEE Aerospace Conference*, 2004, pp. 2667–2679.

[2] Hughes, S. P., "Preliminary Optimal Orbit Design for the Laser Interferometer Space Antenna (LISA)," *AAS Rocky Mountain Guidance and Control Conference*, 2002, pp. 61–78.

[3] Scharf, D. P., Hadaegh, F. Y., and Ploen, S. R., "A Survey of Spacecraft Formation Flying Guidance and Control (Part I): Guidance," *Proceedings of the American Control Conference*, Jun. 2003, pp. 1733–1739.

[4] Scharf, D. P., Hadaegh, F. Y., and Ploen, S. R., "A Survey of Spacecraft Formation Flying Guidance and Control (Part II): Control," *Proceedings of the American Control Conference*, Jun. 2004, pp. 2976–2984.

[5] Chung, S.-J., Ahsun, U., and Slotine, J.-J. E., "Application of Synchronization to Formation Flying spacecraft: Lagrangian Approach," *Journal of Guidance, Control, and Dynamics*, Vol. 32, No. 2, Mar.-Apr. 2009, pp. 512–526.

[6] Schaub, H., Vadali, S. R., Junkins, J. L., and Alfriend, K. T., "Spacecraft Formation Flying Control using Mean Orbital Elements," *Journal of the Astronautical Sciences*, Vol. 48, No. 1, Jan.-Mar. 2000, pp. 69–87.

[7] Vadali, S. R., Alfriend, K. T., and Vaddi, S., "Hill's Equations, Mean Orbital Elements, and Formation Flying of Satellites," *Advances in the Astronautical Sciences*, Vol. 106, 2000, pp. 187–203.

[8] Afriend, K. T., Vadali, S. R., and Schaub, H., "Formation Flying Satellites: Control by an Astrodynamicist," *Celestial Mechanics and Dynamical Astronomy*, Vol. 81, 2001, pp. 57–62.

[9] Schaub, H. and Alfriend, K. T., "J_2 Invariant Relative Orbits for Spacecraft Formations," *Celestial Mechanics and Dynamical Astronomy*, Vol. 79, 2001, pp. 77–95.

[10] Breger, L., How, J. P., and Alfriend, K. T., "Partial J_2-Invariance for Spacecraft Formations," *Proceedings of the AIAA Guidance, Navigation and Control Conference and Exhibit*, Aug. 2006.

[11] Breger, L. and How, J. P., "Gauss's Variational Equation-Based Dynamics and Control for Formation Flying Spacecraft," *Journal of Guidance, Control, and Dynamics*, Vol. 30, No. 2, Mar.-Apr. 2007, pp. 437–448.

[12] Hadaegh, F. Y., Chung, S.-J., and Manaroha, H., "Development and Flight of Swarms of 100-gram Class Satellites," *IEEE Systems Journal (to be submitted)*, 2011.

[13] Clohessy, W. and Wiltshire, R., "Terminal Guidance System for Satellite Rendezvous," *Journal of Astronautical Sciences*, Vol. 27, No. 9, 1960, pp. 653–658.

[14] Tschauner, J. and Hempel, P., "Rendezvous Zu Einem In Elliptischer Bahn Umlaufenden Ziel," *Acta Astronautica*, Vol. 11, No. 2, 1965, pp. 104–109.

[15] Schweighart, S. and Sedwick, R., "High-Fidelity Linearized J_2 Model for Satellite Formation Flight," *Journal of Guidance, Control, and Dynamics*, Vol. 25, No. 6, Nov.-Dec. 2002, pp. 1073–1080.

[16] Hamel, J.-F. and Lafontaine, J. D., "Linearized Dynamics of Formation Flying Spacecraft on a J_2-Perturbed Elliptical Orbit," *Journal of Guidance, Control, and Dynamics*, Vol. 30, No. 6, Nov.-Dec. 2007, pp. 1649–1658.

[17] Gim, D. and Alfriend, K., "State Transition Matrix of Relative Motion for the Perturbed Noncircular Reference Orbit," *Journal of Guidance, Control, and Dynamics*, Vol. 26, No. 6, Nov.-Dec. 2003, pp. 956–971.

[18] Xu, G. and Wang, D., "Nonlinear Dynamic Equations of Satellite Relative Motion Around an Oblate Earth," *Journal of Guidance, Control, and Dynamics*, Vol. 31, No. 5, Sep.-Oct. 2008, pp. 1521–1524.

[19] Chang, I., Chung, S.-J., and Blackmore, L., "Cooperative Control with Adaptive Graph Laplacians for Spacecraft Formation Flying," *49th IEEE Conference on Decision and Control*, Atlanta, GA, December 2010, pp. 4926–4933.

[20] Acikmese, B., Bayard, D. S., and Hadaegh, F. Y., "On the Evolution of Orbiting Spacecraft Swarms," *Jet Propulsion Lab, Internal Document (in preparation)*, 2011.

[21] Chang, I., Chung, S.-J., and Hadaegh, F., "Phase Synchronization Control of Robotic Networks on Periodic Ellipses with Adaptive Switching Topologies," *AIAA Guidance, Navigation, and Control Conference (accepted)*, Portland, OR, August 2011.

[22] Kechichian, J. A., "Motion in General Elliptic Orbit with respect to a Dragging and Precessing Coordinate Frame," *Journal of the Astronautical Sciences*, Vol. 46, No. 1, Jan.-Mar. 1998, pp. 25–45.

American Institute of Aeronautics and Astronautics